NASA-CR-199721

The Control of Purity and Stoichiometry of Compound Semiconductors by High Vapor Pressure Transport

Final Report on NASA Grant NAGW-2865

Klaus J. Bachmann
Department of Materials Science and Engineering
and
Kazufumi Ito, Jeffery S. Scroggs, and Hien T. Tran
Center for Research in Scientific Computation, Department of Mathematics
North Carolina State University, Raleigh, North Carolina 27695-7919

Abstract

In this report we summarize the results of a three year research program on high pressure vapor transport (HPVT) of compound semiconductors, ~~funded by NASA Grant NAGW-2865.~~ Most of our work focused onto pnictides, in particular $ZnGeP_2$, as a model system. Access to single crystals of well controlled composition of this material is desired for advancing the understanding and control of its point defect chemistry in the context of remote, real-time sensing of trace impurities, e.g. greenhouse gases, in the atmosphere by $ZnGeP_2$ optical parametric oscillators (OPOs). The report is presented in 9 parts addressing

1. Background information concerning the motivations for our research
2. Experimental arrangements for high pressure vapor transport
3. Identification of transport reactions and thermochemical calculations
4. Phase equilibria and transport conditions
5. Estimation of physico-chemical parameters for the modeling of HPVT
6. Modeling of flow under the conditions of HPVT
7. Characterization of crystal properties
8. Point defect chemistry and physical properties
9. Interactions and presentations

A comprehensive assessment of the current status of the art and science and $ZnGeP_2$ crystal growth and characterization was carried out as part of an international workshop held in Vesser, Germany, August 21-26, 1995[1]. A brief summary of the results of this workshop is included as an addendum to this report (attachment A-1).

1. Introduction

The transport of transparent crystals of $ZnGeP_2$ in a temperature gradient using a liquid source was discovered by Xing et al. in 1989[2] and suggested superior optical properties, that is, lower residual absorption in the transparency range below the fundamental absorption edge than for melt-grown single crystals of the same material. This is of interest in remote detection, for example, in the context of continuous emission monitoring (CEM) devices, relying on continuously tunable infrared lasers, such as, $ZnGeP_2$ optical parametric oscillators (OPOs). Minimum absorption is essential in this application for optimizing the laser damage threshold and the efficiency of frequency conversion. The bandgap (~2.2 eV) and infrared absorption edge (~0.1 eV) of $ZnGeP_2$ makes it possible to cover the wavelength regime between 2-13 μm where many fundamental rotational-vibrational molecular states are found. At present, the fabrication of $ZnGeP_2$ OPOs is based on bulk single crystals grown from the melt for which, in spite of 25 years of research and development, the absorption behavior is still poorly understood. Our research concerning the HPVT growth of $ZnGeP_2$ crystals and their characterization aims at improving this situation by the generation of standards of well defined point defect chemistry - based on the far more sensitive control of the solidus composition by the control of partial pressures of the constituents during vapor growth than possible under the conditions of growth from the melt.

2. Experimental conditions of HPVT

Figure 1(a) - (c) show schematically the experimental arrangements used thus far for the study of HPVT growth in our laboratory. The arrangement used by Xing et al.[2] is shown in fig. 1(a) and involved transport in a shallow vertical temperature gradient from molten $ZnGeP_2$ that is contained in a pyrolytic BN boat to the wall of the fused silica enclosure. Subsequent studies employed a zone melting geometry that allowed growth from a moving molten source zone established in a bar of $ZnGeP_2$ thus minimizing changes in the composition of the transported crystals due to depletion of the melt in the course of the growth process. A typical crystal obtained in this way is shown in figure 2[3]. It is transparent and of bright red collor. On its surface it exhibits a set of macrosteps due to step bunching in the course of the growth process. A third arrangement is similar to that described by Scholz[4] and employs a ring shaped source heated by glow bars to temperature T_s with transport to a window on the bottom of the fused silica enclosure held at temperature T_c[5] (see attachment A-2). The regions above and below the glow bar position are kept at constant temperature T_i by means of two isothermal furnace liners filled with sodium vapor and the window is cooled by a jet of nitrogen gas to establish

well controlled thermal conditions. A booster heater is inserted in the top well of the enclosure to permit fine tuning of the temperature T_p.

3. Identification of the transport reaction and thermochemical calculations

The partial pressures of P_2/P_4 vapor and zinc over $ZnGeP_2$ have been established through preceding work[6]-[8] and are shown as a function of temperature in table 1. To our knowledge the nature of the Ge vapor species participating in the transport reaction has not been addressed in the literature. The vapor pressure over pure germanium in the temperature range of $ZnGeP_2$ HPVT is well known, that is, $\leq 2x10^{-8}$ bar at $T \leq 1300K$. Since the partial pressure of atomic Ge vapor over molten $ZnGeP_2$ is expected to be less than that over pure Ge at the same temperature the observed transport rates, typically $5x10^{-6}$ mole/m^2s, cannot be explained in terms of atomic germanium vapor playing a significant role in the transport reaction. Therefore, molecular Ge containing species must be present in the vapor phase. A possible source for the generation of such volatile molecular species is residual oxygen. Thermochemical calculations using the Chemsage code[9] were carried out, for the oxygen partial pressure expected on the basis of (in decreasing order of importance): (i) oxygen diffusion through the fused silica wall of the growth capsule, (ii) outgasing of residual water from the silica walls and (iii) reaction of the vapor atmosphere with the inner wall of the capsule. They predict a partial pressure of GeO(g) of $10^{-12}<p_{GeO}<10^{-9}$ in the temperature range $1100K \leq T \leq 1300K$[10] (see attachment A-3 for details). However, cutting off the supply of oxygen by diffusion through the fused silica wall by the use of nitrogen jacketed fused silica ampules, and reducing out-gasing as a source of oxygen by a careful vaccum bake of the growth capsules, does not significantly reduce the transport rate.

Thus the observed efficient transport must be explained by an alternative transport mechanism, that is, molecular Ge_xP_y must be present in the vapor phase over molten $ZnGeP_2$. This is corroborated by optical absorption spectroscopy[11]. Figure 3 shows a schematic representation of the experimental arrangement used by us for this study. Fused silica cuvettes ranging from 50 to 100 mm length and 10 mm diameter, containing red phosphorus as well as $ZnGeP_2$, ZnP_2 and GeP, respectively, were heated in a furnace - equipped with isothermal furnace liners to establish a uniform temperature over the length of the cuvettes. The absorption spectra for the vapor atmosphere above these materials were measured in the range $180 \leq \lambda \leq 1\,\mu m$. The details of the measurements and resulting spectra for the four materials investigated at $\lambda \leq 350nm$ are given in the attached reprint A-4 of ref. 11. A comparison of the spectra for the three compounds under study shows spectral lines associated with vibronic transitions in the vapor phase

above $ZnGeP_2$ that cannot be explained by the absorption lines for either P_2, P_4, Zn, their oxides or GeO.

Table 2 shows the position of the lines associated with Ge_xP_y in comparison to spectral lines associated with P_2. Although the resolution of our spectrometer is not sufficient to allow an unequivocal identification of the stoichiometry of the Ge_xP_y vapor species, based on the limited number of known Ge-P compounds, we identify it tentatively as GeP, which is presently being further investigated by mass spectrometric analysis. Thus the reactions

$$Zn(g) + GeP(g) + 1/2P_2(g) \Leftrightarrow ZnGeP_2(s)$$

and

$$Zn(g) + GeP(g) + 1/4P_4(g) \Leftrightarrow ZnGeP_2(s)$$

are chosen to describe the overall transport.

4. Phase equilibria and transport conditions

Figure 4 shows the Gibbs phase triangle for the system Zn-Ge-P. Of the Ge-P compounds shown on the Ge-P binary only GeP, and possibly GeP_2, exist at 1 bar pressure. GeP_3 and GeP_5 can only be prepared at very high pressure (65kbar)[12]. On the Zn-P binary two compounds, Zn_3P_2 and ZnP_2 exist at 1bar pressure. Using the thermochemical data of table 3, the predominance field for $ZnGeP_2$ has been calculated and is shown in fig. 5 for two temperatures that are relevant for the execution of HPVT crystal growth. Note that the limit at very high phosphorus pressure is not well defined by the calculation. However within the range of phosphorus pressures used in our experiments the width of the predominance field $ZnGeP_2$ clearly decreases with decreasing temperature and the limits of the predominance field shift toward smaller Zn pressures. Also, the predominance fields shown in fig. 5 allow ZnP_2, Zn_3P_2 and $ZnGeP_2$ or Zn_3P_2, Ge and $ZnGeP_2$ to coexist in equilibrium.

Table 4 shows the results of transport experiments employing $ZnGeP_2$ charges plus various additions, e.g., O_2, phosphorus, ZnP_2, and Zn_3P_2, respectively. Also, the temperatures of the source and of the growing crystal was varied within the ranges 1301K $\leq T_S \leq$ 1315K and 1248K$\leq T_C \leq$ 1280K. Shallow temperature gradients (~4K/cm) and short transport distances are required for single phase transport by HPVT. Thus the vertical transport observed in ref. 1 corresponds to close to ideal conditions. Also, a set of experiments was conducted metering well controlled amounts of HCl gas into the growth capsule to enhance the Ge-concentration in the vapor phase. Halide transport of $ZnGeP_2$

has been utilized by others[13] for homoepitaxial growth on $ZnGeP_2$ substrates of (100), (001) and (112) orientation according to the transport equation

$$2Zn(g) + P_2(g) + GeCl_2(g) \Leftrightarrow ZnGeP_2(s) + ZnCl_2.$$

Single phase $ZnGeP_2$ HCl transport is attained for a typical composition of 6.27×10^{-7} mole/cm^3 of zinc, 3.254×10^{-5} mole/ cm^3 phosphorus and 1.3×10^{-5} mole/cm^3 HCl.

5. Estimation of physico-chemical parameters for the modeling of HPVT

The relative importance of convective and diffusive transport in HPVT is captured by the solutal Peclet number that is defined as

$$Pe_d = \frac{v_c \bullet l_c}{D}$$

where v_c, l_c, and D represent the linear flow velocity, a characteristic length scale, in this case the diameter of the vortices, and diffusivity. The flow is characterized by the Reynolds number

$$Re = \frac{\rho v_c l_c}{\eta} \quad ,$$

where ρ is the vapor density and η is the kinematic viscosity. For large values of the Peclet number boundary layers form and the transport becomes diffusion limited. Under conditions of laminar flow, that is, $Re < 2100$, the width of the boundary layer is proportional to $1/\sqrt{Re}$.

Based on a preceding evaluation of the second virial coefficient for phosphorus vapor[14], in the pressure range considered for HPVT of $ZnGeP_2$ deviations from ideal behavior are small so that the kinetic theory of gases provides valid order of magnitude estimates of D and η. At 1300K, the vapor atmosphere over $ZnGeP_2$ consists of approximately 2.77 bar of P_2 and .38 bar of P_4 corresponding to a mass density $\rho = 5.17$ kgm^{-3}. The sum of the radii of P_2 and P_4 $r_{P2\text{-}P4} = 5.2 \times 10^{-10}$m resulting in $\sigma = 8.5 \times 10^{-19}$ m^2 and $\lambda = kT/\sqrt{2}\sigma p = 4.75 \times 10^{-8}$ m. With reduced molecular mass $m_r \approx 6.9 \times 10^{-26}$ kg the mean molecular speed $c_{av} = (8kT/\pi m_r)^{1/2} = 814$ ms^{-1}, that is, $\eta \approx (n m_r \lambda c_{av} N_L)/3V \approx 1.56 \times 10^{-5}$ kgm^{-1}s^{-1} and $D_{P2/P4} \approx \lambda c_{av}/3 \approx 1.29 \times 10^{-5}$ m^{2}s^{-1}. The heat capacity at constant pressure $C_p = 606$ Jkg^{-1}K^{-1} $\kappa_t \approx (n \lambda c_{av} C_v)/3 \approx 0.227$ JK^{-1}s^{-1}m^{-1}. Also, under the

conditions of our experiments, $l_c \approx 10^{-2}$ m and $v_c \approx 5x10^{-2} ms^{-1}$, so that Pe(ideal gas) ≈ 39 and Re(ideal gas) ≈ 172.

Using corrections for molecular interactions in the computations of the viscosity, thermal conductivity, and diffusivity[15, 16] $\eta = 2.69x10^{-5}$ $kgm^{-1}s^{-1}$ (269 micropoise), $\kappa_t = 2.30x10^{-2}$ $JK^{-1}s^{-1}m^{-1}$ and $D_{P_2P_4}(1300K) = 2.26x10^{-5}$ m^2s^{-1}. Thus $Pe_d = 22.1$ and Re = 96, that is, for the case of $ZnGeP_2$, both convective and diffusive transport have to be considered, but the flow can be expected to be laminar, which simplifies the computations. In order to take into account the temperature variations in the HPVT enclosure we consider next the Rayleigh number

$$Ra = \frac{\rho^2 g \alpha_t C_p \Delta T}{\eta \kappa_t}$$

with regimes of flow

laminar:	$Ra \leq 10^8$
transitional:	$10^8 < Ra < 10^{10}$
turbulent:	$Ra > 10^{10}$

Under the conditions of our $ZnGeP_2$ experiments, that is $\Delta T = 80$ K and the volume expansion coefficient $\alpha_t \approx nR/p = 2.64x10^{-5}$ m^3K^{-1}. Thus $Ra = 1.12x10^5$ so that the previous prediction regarding the flow based on the Reynolds number holds. Although for $ZnGeP_2$ the flow thus is predicted to be laminar more detailed numerical calculations are needed for its quantitative characterization under the conditions of HPVT experiments with the specific thermal boundary conditions for the geometries represented in Fig. 1, taking into account the thermal properties of the fused silica enclosures (κ_t = 1.381 Js^{-1} $m^{-1}K^{-1}$).

6. Modeling of the flow and real-time process monitoring

The mathematical model for transport processes in chemical vapor deposition are described by conservation of mass

$$\frac{\partial(\rho)}{\partial t} + \frac{\partial(\rho u)}{\partial x} + \frac{\partial(\rho u)}{\partial y} + \frac{\partial(\rho u)}{\partial z} = 0,$$

conversation of momentum in x

$$\frac{\partial(\rho u)}{\partial t} + \frac{\partial(\rho uu)}{\partial x} + \frac{\partial(\rho uv)}{\partial y} + \frac{\partial(\rho uw)}{\partial z} = -\frac{\partial p}{\partial t} + \frac{\partial}{\partial x}\left[\frac{4}{3}\eta\frac{\partial u}{\partial x} - \frac{2}{3}\eta\frac{\partial v}{\partial y} - \frac{2}{3}\eta\frac{\partial w}{\partial z}\right] + \frac{\partial}{\partial y}\left[\eta\frac{\partial u}{\partial y} + \eta\frac{\partial v}{\partial x}\right] + \frac{\partial}{\partial z}\left[\eta\frac{\partial u}{\partial z} + \eta\frac{\partial w}{\partial x}\right],$$

conservation of momentum in y

$$\frac{\partial(\rho u)}{\partial t} + \frac{\partial(\rho vu)}{\partial x} + \frac{\partial(\rho vv)}{\partial y} + \frac{\partial(\rho vw)}{\partial z} = -\frac{\partial p}{\partial t} + \frac{\partial}{\partial x}\left[\frac{4}{3}\eta\frac{\partial v}{\partial y} - \frac{2}{3}\eta\frac{\partial u}{\partial x} - \frac{2}{3}\eta\frac{\partial w}{\partial z}\right] + \frac{\partial}{\partial x}\left[\eta\frac{\partial v}{\partial x} + \eta\frac{\partial u}{\partial y}\right] + \frac{\partial}{\partial z}\left[\eta\frac{\partial v}{\partial z} + \eta\frac{\partial w}{\partial y}\right],$$

conservation of momentum in z

$$\frac{\partial(\rho w)}{\partial t} + \frac{\partial(\rho wu)}{\partial x} + \frac{\partial(\rho wv)}{\partial y} + \frac{\partial(\rho ww)}{\partial z} = -\frac{\partial p}{\partial t} + \frac{\partial}{\partial x}\left[\frac{4}{3}\eta\frac{\partial w}{\partial z} - \frac{2}{3}\eta\frac{\partial u}{\partial x} - \frac{2}{3}\eta\frac{\partial v}{\partial y}\right] + \frac{\partial}{\partial x}\left[\eta\frac{\partial w}{\partial x} + \eta\frac{\partial u}{\partial z}\right] + \frac{\partial}{\partial y}\left[\eta\frac{\partial v}{\partial z} + \eta\frac{\partial w}{\partial y}\right] - \rho g,$$

conservation of enthalpy H

$$\frac{\partial(\rho H)}{\partial t} + \frac{\partial(\rho uH)}{\partial x} + \frac{\partial(\rho vH)}{\partial y} + \frac{\partial(\rho wH)}{\partial z} = \frac{\partial}{\partial x}\left[\frac{\kappa_t \partial H}{C_p \partial x}\right] + \frac{\partial}{\partial y}\left[\frac{\kappa_t \partial H}{C_p \partial y}\right] + \frac{\partial}{\partial z}\left[\frac{\kappa_t \partial H}{C_p \partial z}\right],$$

and diffusive transport of species B in mixture A, B with mass fractions f_A, f_B

$$\frac{\partial(\rho f_B)}{\partial t} + \frac{\partial(\rho u f_B)}{\partial x} + \frac{\partial(\rho v f_B)}{\partial y} + \frac{\partial(\rho w f_B)}{\partial z} = \frac{\partial}{\partial x}\left[\rho D_{AB}\frac{\partial f_B}{\partial x}\right] + \frac{\partial}{\partial y}\left[\rho D_{AB}\frac{\partial f_B}{\partial y}\right] + \frac{\partial}{\partial z}\left[\rho D_{AB}\frac{\partial f_B}{\partial z}\right] + \frac{\partial}{\partial x}\left[\rho D_{AB}\alpha_T f_A f_B\frac{\partial \log T}{\partial x}\right] + \frac{\partial}{\partial y}\left[\rho D_{AB}\alpha_T f_A f_B\frac{\partial \log T}{\partial y}\right] + \frac{\partial}{\partial z}\left[\rho D_{AB}\alpha_T f_A f_B\frac{\partial \log T}{\partial z}\right]$$

Based on the conservation of mass it can be shown that

$$\int_{\Omega_t} \left[\frac{\partial}{\partial t} \rho + \mathrm{div}(\rho \mathbf{u}) \right] \quad dV = 0$$

for any domain Ω_t of the gas phase. Thus the integrand must vanish in accord with the conservation of mass equation given above. For incompressible fluids this reduces to

$\mathrm{div}(\mathbf{u}) = 0$. All buoyancy effects are included in the model through the gravitational term in the Navier-Stokes (momentum) equations that are based on Stokes' hypothesis relating the shear viscosity to the bulk viscosity so that the viscosity can be represented by a single parameter η[16]. Also, body force enters into the transport model through the momentum equations and the separation of gas species due to different size and mass is modeled by the terms $\partial/\partial\xi[\rho D_{AB}\alpha_T f_A f_B \partial \log T/\partial\xi]$ in the transport equation, where α_T is the thermal diffusion constant. In the Boussinesq approximation[17], the density is assumed to be a constant in all equations except for the existence of a buoyancy force in the presence of a gravitational field due the density variations related to thermal expansion, representing the body force term $\rho\mathbf{g}$ as $\rho[1 - \beta_T(T-T_{ref})\mathbf{g}$, where$\rho$ is a constant, β_T is the thermal volume expansion coefficient and T_{ref} is the reference temperature.

The coupled set of non-linear differential equations thus defined was solved numerically for a range of parameters which include: reactor geometry, operating pressure, gravitational vector, and the parameters evaluated in section 5, that is, κ_t, η, ρ, and C_v. Two fluid dynamics packages, FLUENT, a finite difference code, and FIDAP, a finite element code, were licensed for the simulation study. Due to the ability to model more complex geometries the FIDAP package was found to be more versatile for our work and most of the computations were based on this code. Initially the flow dynamics of a homogeneous gas inside a closed ampule of fused silica was modeled numerically for axi-symmetrical conditions using quadratic-triangular meshes. The numerical simulations were performed to study the flow dynamics and temperature distribution inside the fused silica ampule and to illustrate the feasibility of an optimal reactor design study. Several parameter studies were caried out . The problem governed by the coupled set of partial nonlinear differential equations was simulated for a range of parameters with a view to maximizing transport and uniformity of deposition. These parameters include: reactor geometry, aspect ratio, operating pressure, gravitational vector, thickness of the fused silica window and boundary temperature profiles. The parameter studies indicate thet the best configuration has the substrate on the bottom and that flow rate increases with increase in pressure[18-20]. In addition, conditions for optimum convective mixing at the source and transport to the seed crystal in a closed ampule high pressure vapor transport were obtained, and led to changes in the design, including the location of the heating element[5].

In addition to the parameter studies, a more rigorous approach to the optimal design and control has been taken. In ref. 20 the experimental design problem was formulated as a shape optimization problem with respect to the geometry of the reactor and a boundary temperature control problem. The material and shape derivatives of

solutions to the Boussinesq approximation were derived. Optimality conditions and a numerical optimization method based on the augmented Lagrangian method were developed for boundary control of the Boussinesq flow. The regularity of solutions has also been studied. In ref. 21; well-posedness and necessary optimality conditions for optimal control problems for homogeneous incompressible gas flow inside a HPVT ampule by boundary temperature control was studies. A second order method based on an augmented Lagrangian formulaton was applied to solve the optimal control problem for the steady flow. Our numerical calculations indicate the effectiveness of temperature control through a portion of the boundary for improving the vertical transport flow inside the ampule.

The modeling was then further advanced to permit the investigation of non-axi-symmetric geometries where 3-dimensional modeling must be applied[22] (see attached preprint A-4b for details). The latter is mandatory in the context of real-time optical monitoring of the growth process for which we introduced a new method that is highly sensitive with regard to both the initial phase of nucleation and late stages of three dimensional growth[23]. This method, p-polarized reflectance spectroscopy (PRS), is based on the changes in the reflectance of the overgrowth of a substrate with regard to a beam of p-polarized light that impinges onto the surface at the Brewster angle of the substrate as illustrated in Fig. 7 for the overgrowth of a seed crystal plate (e.g., a wafer of silicon) - located on the cooled fused silica window of the growth ampule depicted in Fig. 1(c) - by a crystal layer (e.g., $ZnGeP_2$). The reflected beam is detected by a photodiode, processed through a phase sensitive amplifier and read into a computer.

The complex reflectivity r of a three-layer stack composed of materials labeled a, c and s for ambient, crystal and seed, respectively, with interfaces labeled ac and cs, is given by

$$r = \frac{r_{ac} + r_{cs}\exp(-i\Phi)}{1 + r_{ac}r_{cs}\exp(-i\Phi)}$$

with reflectivity coefficients

$$r_{ac} = \frac{\varepsilon_c \cos\varphi_o - \sqrt{\varepsilon_a}\sqrt{\varepsilon_c - \varepsilon_a \sin^2\varphi_o}}{\varepsilon_c \cos^2\varphi_o + \sqrt{\varepsilon_a}\sqrt{\varepsilon_c - \varepsilon_a \sin^2\varphi_o}}$$

$$r_{cs} = \frac{\varepsilon_s\sqrt{\varepsilon_c - \varepsilon_a \sin^2\varphi_o} - \varepsilon_c\sqrt{\varepsilon_s - \varepsilon_a \sin^2\varphi_o}}{\varepsilon_s\sqrt{\varepsilon_c - \varepsilon_a \sin^2\varphi_o} + \varepsilon_c\sqrt{\varepsilon_s - \varepsilon_a \sin^2\varphi_o}}$$

and phase

$$\Phi = \frac{2\pi t_c}{\lambda}\sqrt{\varepsilon_c - \varepsilon_a \sin^2\varphi_o} \quad ,$$

where ε_a, ε_c, and ε_s refer to the dielectric functions at the energy of the incident laser beam of the ambient, the crystal and the seed assuming that reflections at the seed crystal interface with the cooled fused silica window can be neglected. Due to constructive and destructive interference between the partial waves reflected at the crystal/seed and ambient/crystal interfaces, upon initiation of growth the reflected intensity $R_p = rr^*$ oscillates between maxima and minima the distance of which in time is uniquely related to the phase thickness of the growing crystal layer that enters into the periodic exponential function in the equation for r (see Figure 8 for a simulation of the growth of various materials on Si). Thus the growth rate should be accessible in real-time if the problems related to beam stirring in a dense vapor atmosphere can be controlled. In addition to providing information regarding the growth rate, a fine structure superimposed on the oscillations due to interference is observed for pulsed vapor deposition processes. The analysis of this fine structure results in detailed information on the kinetics of crystal growth that is, on the properties of the surface reaction layer that connects the growing film to the nutrient vapor phase. Initial simulations of this four-layer stack have been carried out for the growth of GaP on Si[24] (see Attachment A-10).

In order to assess this problem for the conditiond of HPVT of $ZnGeP_2$ numerical calculations of the density variations and the related gradients in the dielectric function of the ambient phase, the vapor, were performed using non-uniform quadrilateral elements for the representation of the 3-D flow in the growth capsule that no longer supports axisymmetric flow. This is due to the alteration of the capsule shown in Fig.1(c) by the provision of two additional optical windows for the implementation of PRS, that is, an entrance port for the laser beam to strike the substrate located on the bottom of the capsule at its Brewster angle and an exit port for the reflected beam that is intercepted by a detector. Under the conditions of close-space vapor transport of $ZnGeP_2$ from top to bottom at the earth's gravity and 10^{-2} **g**, which represents an upper limit for the g-jitter expected for the space shuttle during astronaut activities[22], our computations show that changes in the ampule orientation with regard to the gravity vector affect the temporal gradients by less 16% at 1**g** and <1% at 10^{-2}**g**. Thus only moderate reductions of the gravity vector are needed for this type of experimentation and astronaut activities do not impose a significant limitation to their successful excecution.

An assessment of the problems associated with beam stirring in the context of real-time optical process monitoring was made on the basis of combining Snell's law

$$n_1 \sin\varphi_1 = n_2 \sin\varphi_2$$

and the Dale-Gladstones law

$$n_i = h\rho_i + 1$$

with Dale-Gladstone constant $h = 2.26 \times 10^{-4}\ m^3 kg^{-1}$ to compute the deviation of the angle from normal incidence at the entrance window along a path inside the growth capsule - divided into 26 segments ending at the point of reflection on the substrate wafer. The result is shown in Fig. 9 and indicates that beam bending in the relatively steep temperature gradient close to the substrate surface may affect the sensitivity and accuracy of the method. However, calculations - based on a reliable parameter set - can provide for corrections that restore high sensitivity and accuracy by appropriate compensation of the entrance angle. Also, the problem of noise due to random time-dependent fluctuations of the vapor density can be largely eliminated by phase-sensitive detection so that with sufficient computational support PRS would be a reliable method for remote real-time sensing of crystal growth processes on earth and in space for a wide range of vapor pressures.

7. Characterization of crystal properties

Figure 10 shows steady state photoluminescence (PL) spectra for (a) $ZnGeP_2$ platelets grown by the HPVT method and (b) $ZnGeP_2$ plates cut from a bulk single crystal grown by the gradient freezing method with and without annealing and etching. All exhibit in the as-grown state broad infrared emission peaked at 1.3 eV[25]. The PL spectra for a crystal grown by HPVT from a nearly stoichiometric melt in a shallow gradient, in addition to deep luminescence, exhibit near edge emission. For bulk single crystals grown by the gradient freezing method, near edge emission is absent. However, a high energy shoulder is observed in the dominant deep emission extending to ~1.7 eV. Subband excitation extending to 1.6 eV are also observed for these crystals in the photoconductivity (PC) spectra. Annealing in vacuum at 500°C for 400 hrs results in a substantial increase of the 1.7 eV emission relative to the 1.3 eV emission. Also, a significant reduction in the near infrared absorption is observed upon annealing.

Figure 11 shows the time dependence of the PL, which cannot be described by exponential functions, that is, the PL intensity has a hyperbolic dependence on time[26]. Thus the PL spectra are dominated by donor-acceptor transitions that are associated with time constants depending on the relative spacing of the donors and acceptors in the lattice.

Figure 12 shows an interpretation of all optical data known todate the position of energy eigenvalues and subbands in the bandgap of $ZnGeP_2$ that are associated with residual donor and acceptor states. For example, the broad PL band, peaked at 1.3 eV, is attributed to transitions between filled acceptor (A1) and unfilled donor (D1) states that are associated with subbands having a center distance of 1.3 eV. Explaining the sub-bandgap structure in the PC spectra by transitions between filled A1 states and the conduction band edge (CBE), the highest filled A1 state is associated with an energy eigenvalue ~1.6 eV below the CBE. The region of residual absorption within the transparency range of $ZnGeP_2$ extends from the absorption edge to well below 1.6 eV, due to transitions between filled acceptor and empty donor states that do not contribute to the PC spectra because of the high effective mass in the donor subbands.

There are at least three effects that must be considered in the interpretation of the annealing studies: (i) The reduction of quenched-in disorder, reducing the concentration of point defects. (ii) The shift of the FL position associated with this annihilation of defects, altering the population of the remaining defect states. (iii) Shifts in the FL position caused by the generation of defects at the crystal surface upon annealing. The observation of additional structure in the PL and the depth dependence of the luminescence features after annealing clearly establishes the latter and requires the consideration of additional donor-acceptor energy subband transitions.

8. Point defect chemistry and physical properties

For the above mentioned thermal conditions and partial pressures, at the onset of the HPVT experiment, the supersaturation at the substrate location corresponds to zinc and phosphorus supersaturated growth conditions. However, upon prolonged HPVT growth without melt replenishment, the gradual depletion of the source of zinc causes conversion to Zn-deficient growth conditions that may result in the formation of a Ge-rich second phase on the surface of the $ZnGeP_2$ crystals in extreme cases. The changes in the point defect chemistry accompanying the transitions from maximum to minimum zinc activity in the solid are reflected in the optical properties of the $ZnGeP_2$ crystals. Thus the gradual transitions from the border of the homogeneity range about $ZnGeP_2$ corresponding to maximum zinc activity to the border corresponding to maximum Ge activity during growth confirms our initial premise that HPVT permits the control of stoichiometry over the entire existence range of $ZnGeP_2$.

Point defects that may be generated upon deviation of the ternary compound composition from stoichiometric $ZnGeP_2$ are Zn , Ge and P vacancies - denoted by V_{Zn}, V_{Ge} and V_P - and various antisite defects, e.g., Ge on Zn sites denoted by Ge_{Zn}. Note that

Figure 12 shows an interpretation of all optical data known todate the position of energy eigenvalues and subbands in the bandgap of $ZnGeP_2$ that are associated with residual donor and acceptor states. For example, the broad PL band, peaked at 1.3 eV, is attributed to transitions between filled acceptor (A1) and unfilled donor (D1) states that are associated with subbands having a center distance of 1.3 eV. Explaining the sub-bandgap structure in the PC spectra by transitions between filled A1 states and the conduction band edge (CBE), the highest filled A1 state is associated with an energy eigenvalue ~1.6 eV below the CBE. The region of residual absorption within the transparency range of $ZnGeP_2$ extends from the absorption edge to well below 1.6 eV, due to transitions between filled acceptor and empty donor states that do not contribute to the PC spectra because of the high effective mass in the donor subbands.

There are at least three effects that must be considered in the interpretation of the annealing studies: (i) The reduction of quenched-in disorder, reducing the concentration of point defects. (ii) The shift of the FL position associated with this annihilation of defects, altering the population of the remaining defect states. (iii) Shifts in the FL position caused by the generation of defects at the crystal surface upon annealing. The observation of additional structure in the PL and the depth dependence of the luminescence features after annealing clearly establishes the latter and requires the consideration of additional donor-acceptor energy subband transitions.

8. Point defect chemistry and physical properties

For the above mentioned thermal conditions and partial pressures, at the onset of the HPVT experiment, the supersaturation at the substrate location corresponds to zinc and phosphorus supersaturated growth conditions. However, upon prolonged HPVT growth without melt replenishment, the gradual depletion of the source of zinc causes conversion to Zn-deficient growth conditions that may result in the formation of a Ge-rich second phase on the surface of the $ZnGeP_2$ crystals in extreme cases. The changes in the point defect chemistry accompanying the transitions from maximum to minimum zinc activity in the solid are reflected in the optical properties of the $ZnGeP_2$ crystals. Thus the gradual transitions from the border of the homogeneity range about $ZnGeP_2$ corresponding to maximum zinc activity to the border corresponding to maximum Ge activity during growth confirms our initial premise that HPVT permits the control of stoichiometry over the entire existence range of $ZnGeP_2$.

Point defects that may be generated upon deviation of the ternary compound composition from stoichiometric $ZnGeP_2$ are Zn , Ge and P vacancies - denoted by V_{Zn}, V_{Ge} and V_P - and various antisite defects, e.g., Ge on Zn sites denoted by Ge_{Zn}. Note that

specific deviations from stoichiometry within the homogeneity range about the exact composition $ZnGeP_2$ does not establish the dominance of a specific native point defect, since combinations of other defects may create the same deviations and interactions with extrinsic point defects must be considered.

However, certain conclusions are possible by the interpretation of the optical characterization results in conjunction with the results of electrical measurements and ESR/ENDOR investigations. For example, $ZnGeP_2$ and $ZnSi_xGe_{1-x}P_2$ epilayers grown by organometallic chemical vapor deposition exhibit a wide range of solid solutions corresponfing to the replacement of a large fraction of the zinc atoms by group IV atoms in metastable equilibrium depending on the zinc to germanium precursor flow rate ratio[27-29]. This is only possible by massive antisite defect formation on both the zinc and phosphorus sublattices. Also, regardless of the as-grown composition, annealing in vacuum depletes the near surface region with regard to the most volatile constituents, that is, phosphorus and zinc. By the mass action law, the formation of vacancies on the zinc sublattice reduces the concentration of Zn_{Ge} acceptors and enhances the concentration of Ge_{Zn} donors according to the reactions [1]: $V_{Zn} + Zn_{Ge} \rightarrow Zn^x$ and [2]: $V_{Zn} + Ge^x \rightarrow Ge_{Zn}$. The introduction of V_P donors at the surface is associated with the formation of and Ge_P acceptors according to the reaction [3]: $V_P + Ge^x \rightarrow Ge_P$, and possibly, but not necessarily, of Zn_P acceptors. Thus the luminescence at 1.6 and 1.7 eV observed in vaccum annealed bulk crystals (see attachment A-12) may be explained tentatively by transitions from V_P donors to V_{Zn} and Ge_P acceptors, respectively. The overall FL shift associated with the generation of V_P and V_{Zn} depends on the values of the equilibrium constants for reactions [1] - [3], which are not known at present. The high p-type conductivity observed upon annealing in zinc vapor, has been explained by Rud as an effect of Zn_P antisite defect formation[32].

A more definitive control of the stoichiometry of $ZnGeP_2$ is obtained by growth under the conditions of HPVT. The thermochemical calculations of the temperature dependence of the existence range of $ZnGeP_2$ show that HPVT of $ZnGeP_2$ from a molten source ties at the lower substrate temperature into solidus compositions close to the boundary between the $ZnGeP_2$ and ZnP_2 of the $ZnGeP_2$ existence range[11]. The n-type conductivity of $ZnGeP_2$ crystals grown under such conditions suggests the formation of relatively shallow donor states that move the FL toward the conduction band edge. Simultaneously emission at 1.8 eV is observed that is neither seen in melt-grown crystals nor for growth from zinc-depleted vapor sources. The high phosphorus pressure used in the HPVT experiments rules out a higher V_P concentration than observed under the conditions of melt growth. Thus the donor responsible for the 1.8 eV emission for HPVT

growth from a zinc supersaturated vapor phase must be associated with a different point defect that does not form under for HPVT growth from zinc-depleted melt compositions. Possible choices are the P_{zn} and P_{Ge} antisite defects of which only the P_{Ge} donor explains the decrease of the intensity of the 1.8 eV emission with decreasing zinc activity in the solid. Therefore, we associate the relatively shallow donor that is formed upon HPVT growth from a phosphorus and zinc supersaturated vapor phase with the P_{Ge} antisite defect.

Further information is gained from the analysis of optical brightening upon annealing of bulk $ZnGeP_2$ crystals grown from the melt in conjunction with the PL results. The broad deep luminescence in $ZnGeP_2$ crystals observed for crystals grown from the melt and zinc-depleted vapor sources is due to close-spaced D-A pairs , corresponding to the broad donor and acceptor subbands. Accepting the interpretation of the ENDOR measurements of ref. 30, the deep acceptor is associated with V_{zn}. By equation 2 it is in turn associated with the Ge_{Zn} antisite defect, so that the Ge_{Zn}-V_{Zn} close-spaced D-A pairs represent a possible choice. The alternative close-pairing V_P-V_{Zn} has been proposed in ref. 31 on the basis of the photo-induced EPR study. Unfortunately the photo-induced EPR emloying HeNe laser radiation probes only a thin surface region of the $ZnGeP_2$ crystal, which is expected to be depleted of Zn and P. Thus the finding of both V_P and V_{zn} by photo-induced EPR, though being in agreement with other evidence refererring to the near surface region, does not necessarily pertain to the optical brightening upon annealing, which is a bulk effect. We prefer the Ge_{Zn} donor since it provides for the simultaneous elimination of V_{Zn} and Ge_{Zn} sites upon annealing according to the reaction [4]: $Ge_{Zn} \rightarrow Ge^x + V_{zn}$ and the mass action law, which may be further enhanced by a simultaneous reduction of cation disorder on the Ge sublattice, that is, Zn_{Ge} according to [5] $Zn_{Ge} + V_{zn} \rightarrow Zn^x$. The associated FL motion toward the conduction band edge that results in the filling of residual deep Ge_{Zn} donor states by electrons further enhances the optical brightening. Of course, the simultaneous elimination of P- and Zn-vacancies upon annealing would be also possible, but there exists no obvious linkage in this case. Additional insights are likely to emerge from the results of irradiation studies that permit the controlled formation of defects and their characterization. Work on this aspect is being continued in the PI's laboratory in collaboration with industrial partners.

9. Interactions and presentations

The execution of this program greatly benefitted from interactions with Dr. Warren Ruderman and Dr. Ilya Tseybak of INRAD, INC at Northvale, NJ and Dr. Sebastian

Fiechter at the Hahn-Meitner Institut Berlin, Germany. Two graduate students Mr. Gary Wood and Mr. Hal Castleberry made valuable contributions to our research. Mr. Wood completed a master thesis in Materials Science and Engineering in 1994 and Mr. Castleberry is expected to complete a PhD thesis in Materials Science and Engineering on HPVT of $ZnGeP_2$ in the spring of 1996. The results of our work on were reported by Dr. Fiechter in a paper entitled "High pressure vapor transport of binary and ternary compound semiconductors" at the 6th International Symposium on Experimental Methods for Microgravity Materials Science, held at San Francisco in 1993. Prof. Bachmann presented an invited paper entitled "Heteroepitaxy of wide-bandgap ternary semiconductors at the 9th International Conference on Ternary and Multinary compounds at Yokohama, Japan in 1993. Prof Tran presented a paper entitled "Modeling of flow dynamics and its impact on the optimal reactor design problem" at the SIAM meeting on the Identification and Control in Systems Governed by Partial Differential in 1993 and an invited paper entitled Gas dynamics and transport in a high-pressure reactor under microgravity conditions" at the 2nd IEEE Mediterranean Symposium on New Directions in Control and Automation, June, 1994 in Chania, Greece. Prof. Ito presented an invited paper entitled "Optimal control of thermally coupled Navier-Stokes equations" at the IMA meeting in 1994. Two additional papers on different aspects of "High pressure vapor transport of $ZnGeP_2$ crystals" were presented by Dr. Fiechter and Prof. Scroggs at the 7th International Symposium on Experimental Methods for Microgravity Materials Science, held at Las Vegas in 1994. On August 25, 1995 a full day of a workshop brought together experts on $ZnGeP_2$ crystal growth and characterization from the US and Europe to critically assess the present status of our knowledge in this field (see attached workshop summary (attachment A-1).

References

1. International Workshop *"The Control of Stoichiometry in Epitaxial Semiconductor Structures"*, K.J. Bachmann, H. Flietner and C.Schwab, organizers, Vesser, Germany, August 21-26, 1995, workshop overview to be published in Materials Science & Engineering B, 1996 (attachment A-1)
2. G.C. Xing, K.J. Bachmann and J.B. Posthill, *"High-Pressure Transport of $ZnGeP_2$"*, Appl. Phys. Lett. **56**, 271 (1990)
3. Gary Wood, *"The Growth of $ZnGeP_2$ Crystals by High Pressure Vapor Transport"*, Masters Thesis, North Carolina State University, 1994

4. H. Scholz, *"Crystal Growth by Temperature Reversal"*, Philips Techn. Reviews **28**, 316 (1967); *"On Crystallization by Temperature-Gradient Reversal"*, Acta Electronica **17**, 69 (1974)
5. K.J. Bachmann, G.-C. Xing, J.S. Scroggs, H.T. Tran, K. Ito, H. Castleberry and G. Wood, *"Heteroepitaxy of Wide Bandgap Ternary Semiconductors"*, Jpn. J. Appl. Phys. **32**, 133 (1993) (attachment A-2)
6. A.S. Borshchevskii and T.M. Shantsovoi, *"Pressure and Composition of the Vapor above Semiconductive $ZnGeP_2$"*, Inorg. Mater. **11**, 1853 (1975)
7. V.B. Lazarev, V.J. Shevchenko, S.F. Marenkin, and G. Magomedgadghiev, *"The Growth of Large Tetragonal CdP_2 and ZnP_2 Crystals"*, J. Crystal Growth **38**, 275 (1977)
8. E. Buehler and J.H. Wernick, *"Phase Relations and Crystal Growth of $ZnGeP_2$"*, J. Crystal Growth **8**, 324 (1971)
9. G. Ericson and K. Hack, *"ChemSage - A Computer Program for the Calculation of Complex Chemical Equilibria"*, Metallurgical Transactions B, **21B**, 1013 (1990)
10. S. Fiechter, H. Castleberry, G. Wood, K.J. Bachmann, H.T. Tran, K. Ito and J.S. Scroggs, *"High Pressure Vapor Transport of Binary and Ternary Compound Semiconductors"*, Proc. 6^h International Symposium on Experimental Methods for Microgravity Materials Science, R. Schiffman, ed., TMS, Warrendale, PA 1994, p. 93 (attachment A-3)
11. S. Fiechter, H. Castleberry, N. Dietz, K.J. Bachmann, H.T. Tran, K. Ito and J.S. Scroggs, *"High Pressure Vapor transport of $ZnGeP_2$: Parameter Evaluation"*, Proc. 7th International Symposium on Experimental Methods for Microgravity Materials Science, R.A. Schiffman, ed., TMS, Warrendale, PA, 1995, p. 57 (attachment A-4)
12. P.C. Donohue, and H.S. Young, *"Synthesis, Structure and Superconductivity of New High Pressure Phases in the System Ge-P and Ge-As"*, J. Solid Stae Chem. **1**, 143 (1970)
13. Yu. G. Kataev, I.A. Bobrovnikova, V.G. Voevodin, E.I. Drigolenko, L.J. Nestryuk and M.P. Yakubenya, *Halide transport of $ZnGeP_2$*, Sov. Phys. J. **31**, 321 (1988)
14. K.J. Bachmann and E. Buehler, *"Phase Equilibria and Vapor Pressures of Pure Phophorus and the In/P System and their Implications Regarding Crystal Growth of InP"*, J. Electrochem. Soc. **121**, 835, 1974

15. R.A. Svela,*"Estimated Viscosities and Thermal Conductivities of Gases at High Temperatures"*, NASA Technical Report TR R-132, NASA, Washington, DC, 1962

16. H. Slichting, Boundary Layer Theory, McGraw-Hill, New York, 1955

17. D.D. Gray and A. Giorgini, *"The Validity of the Boussinesq Approximation for Liquids and Gases"*, Int. J. Heat Mass Transfer 545 (1976)

18. (a) H.T. Tran, J.S. Scroggs and K.J. Bachmann, *"Modeling of Flow Dynamics and Its Impact on the Optimal Reactor Design"*, Identification and Control in Systems Governed by Partial Differential Equations, SIAM Publications, 1994, p. 1-13; (b) H.T. Tran and J.S. Scroggs, "Optimal Control of Fluid Flow in a Vertical Chemical Vapor Deposition Reactor", Proc. 31th IEEE Conf. on Decision and Control, 1992, p. 3405-3409 (attachments A-5a and A-5b)

19. H.T. Banks, K. Ito, J.S. Scroggs, H.T. Tran, K.J. Bachmann, H. Castleberry and S. Fiechter, *Gasdynamics and Transport in a High Pressure Reactor under Microgravity Conditions*, Proc. 2 IEEE Mediteranean Symp. on New Directions in Control and Automation, Maleme-Chania, Crete, Greece, 1995, p. 197-218 (Attachment A-6)

20. K.Ito, H.T. Tran and J.S. Scroggs, *"Mathematical Issues in Optimal Design of a Transport Reactor"*, Proc. IMA Volumes in Mathematics and its Applications, Vol. 68, M Gunzburger, ed., 1995, p. 197-218 (attachment A-7)

21. K.Ito, J.S. Scroggs and H.T. Tran, *"Optimal Control of Themally-Coupled Navier Stokes Equations"*, Progress in Systems and Control Theory, Optimal Design and Control, J. Borggaard et al., eds., 1995, p. 199-214 (attachment A-8)

22. J.S. Scroggs, H.T. Banks, K. Ito, S. Ravindran, H.T. Tran, K.J. Bachmann, R.H. Castleberry and N. Dietz, *"High Pressure Vapor transport of $ZnGeP_2$: Three-Dimensional Simulation of Gasdynamics under Microgravity Conditions"*, Proc. 7th International Synposium on Experimental Methods for Microgravity Materials Science, R.A. Schiffman, ed., TMS, Warrendale, PA, 1995, p. 67 (attachment A-4b)

23. N. Dietz, A. Miller and K.J. Bachmann, *" Real-Time Monitoring of Homo-epitaxial and Heteroepitaxial Processes by Parallel-Polarized Reflectance Spectroscopy"*, J. Vac. Sci. Technol. 13, 153 (1995) (attachment A-9)

24. N. Dietz and K.J. Bachmann, *"P-Polarized Reflectance Spectroscopy: A Highly Sensitive Real-Time Monitoring Technique to Study Surface Kinetics under Steady-State Epitaxial Deposition Conditions"*, Vacuum (1996) in print (attachment A-10)

25. N. Dietz, W.Ruderman, I. Tseyback, G. Wood and K.J. Bachmann, *"Native Defect Related Optical Properties of $ZnGeP_2$"*, Appl. Phys. Lett. **65**, 2759 (1994) (attachment A-11)

26. N. Dietz, W. Busse, H.E. Gumlich, I. Tsveybak, W. Ruderman, G. Wood and K.J. Bachmann, *"Characterization of Native Defects in ZnGeP2 by Time-Resolved Photoluminescence"*, J. Crystal Growth., submitted (attachment A-12)

27 G.C. Xing, K.J. Bachmann, G.S. Solomon , J.B. Posthill and M.L. Timmons, *"Organo-metallic Chemical Vapor Deposition of Epitaxial ZnGeP2 Films on (001) GaP Sub-strates"*, J. Crystal growth **94**, 381 (1989)

28. G.C. Xing, K.J. Bachmann, J.B. Posthill and M.L. Timmons, *"Substrate Effects on the Epitaxial Growth of $ZnGeP_2$ Thin Films by Open tube MOCVD"*, J. Appl. Phys. **69,** 4286 (1991)

29. G.C. Xing, K.J. Bachmann, J.B. Posthill and M.L. Timmons, *"Organometallic Chemical Vapor Deposition and Characterization of $ZnGe_{1-x}Si_xP_2$ Alloys on GaP Substrates"*, J. Crystal Growth **113**, 113 (1991)

30. L.E. Halliburton, G.J. Edwards, M.P. Scripsick, M.H. Rankowsky, P.G. Schunemann and T.M. Pollak, *Electron-nuclear double resonance of the zinc vacancy in $ZnGeP_2$*, Appl. Phys. Lett. **66**, 2670 (1995)

31. N.C. Giles, L.E. Halliburton, P.G. Schunemann and T.M. Pollak, *Photo-induced Electron Paramagnetic Resonance of the Phosphorus Vacancy in $ZnGeP_2$*, Appl. Phys. Lett. 66, 1758 (1995)

32 Yu. V. Rud', *"Optoelectronic Phenomena in Zinc Germanium Phosphide"*, Semiconductors, **28**, 633 (1994)

Table 1
Partial Pressures of Vapor Constituents Over $ZnGeP_2$
based on a Chemsage calculation

Temperature [K]	$P(P_4)$ [bar]	$P(P_2)$ [bar]	P(Zn) [bar]	P(GeP) [bar]	P(Ge) [bar]
1300	3.30	0.43	0.24	0.22	1.9×10^{-8}
1290	2.93	0.38	0.21	0.20	1.4×10^{-8}
1275	2.45	0.31	0.18	0.17	9.4×10^{-9}
1250	1.80	0.21	0.123	0.13	4.6×10^{-9}
1225	1.30	0.15	0.09	0.10	2.2×10^{-9}
1175	0.64	0.06	0.05	0.05	4.6×10^{-10}

Table 2

Positions of Absorption Heads

(absorption lined due to GeP_x + absorption lines of P_2 for reference)

Absorption lines of P_2 in nm	Absorption lines of Ge_xP_y in nm
	III: 190.3, 194.1, 195.4, 197.0, 198.0, 200.0.
	201.5 I
203.6	
205	
205.5	205.35 I
206.9	
207.49	207.58 P
208.83	
209.43	209.8 I, P
210.81	211.07 P
	212.02 I
212.26	
212.86	212.98 P
	213.62
214.3	214.26 P
215.0	
	215.94 II
216.4	216.8 P
	217.78 I, II
218.64	218.74 P
220.14	220.34 I, P
	222.59 II
	223.55 I
226.16 I	226.11 I
	227.08 I
	228.37 II
	231.59 I
232.65	232.55
	234.16 I, II
236.76	236.73 P
	238.98 I
240.99	240.91 P, II
	241.56
	243.2
	244.51 I
	246.77 II

Table 3

Thermochemical Data

(dimensions: standard heats of formation ΔH°_{f}, heats of fusion ΔH_{fu} and heats of evaporation ΔH_{ev} in kcal/mole; standard entropies ΔS°_{f} and molar heat capacities c_p in cal/mole•Kelvin)

Element/ Compound	ΔH_f° ΔH_{fu} ΔH_e	S_f°	$c_p = A+B\cdot10^{-3}\cdot T+C\cdot10^{5}\cdot T^{-2}$ A	B	C
P(red)	0.00	5.45	4.051	3.559	-
P_4(white)	16.68	39.28	18.28	15.12	-
P(l)	17.31	-	25.168	-	T>317 K
P_4(g)	**30.77**	**66.89**	**19.562**	**0.162**	**-3.213**
P_2(g)	**40.68**	**52.11**	**8.675**	**0.191**	**-0.994**
Zn(s)	0.00	9.943	5.096	2.782	0.13
Zn(l)	1.75	-	7.495	-	-
Zn(g)	**31.15**	**38.451**	**4.965**	**-**	**-**
$ZnCl_2$(s)	-99.13	26.62	14.290	8.994	-
$ZnCl_2$(l)	2.474	-	2.588	-	-
$ZnCl_2$(g)	**-63.839**	**66.185**	**14.74**	**-1.03**	**-**
Ge(s)	0.00	7.425	5.577	0.931	-0.25
Ge(l)	8.82		6.596		T>1210 K
Ge(g)	**89.34**	**40.1**	**7.038**	**-0.873**	**0.76**
GeH_4(g)	21.68	51.89	14.939	5.276	-5.166
GeP(s)	**-0.13**	**14.6**	**10.84**	**2.7**	**-1.25**
GeP(g)	**28.4**	**44.43**	**12.34**	**-**	**-**
GeO(s)	-50.3	11.9	9.543	3.497	-
GeO(g)	-10.99	53.49	8.92	0.0239	-1.3685
Ge_2O_2(g)	-112.	75.1	20.	-	-
Ge_3O_3(g)	**-212.**	**99.3**	**32.**	**-**	**-**
GeCl(g)	174.36	58.72	10.314	-0.532	-1.18
$GeCl_2$(g)	**-40.84**	**70.63**	**13.818**	**0.052**	**-0.88**
ZnP_2	**-24.15**	**14.4**	**17.01**	**3.997**	**0.65**
Zn_3P_2	**-38.65**	**36.2**	**30.15**	**6.225**	**-0.36**
$ZnGeP_2$	**-26.3**	**28.22**	**24.65**	**3.5**	**-4.0**

Chemical Transport Experiments in the Parallel Processing Furnace

Transport Method	*Additives*	T_{source} *(K)*	T_{growth} *(K)*	ΔT *(K)*	*Transported Material*	*Transport Rate (mg/hr)*	*Time*	*Ampoule Preparation /Length*
1-1 c Chemical HPVT,	HCl (35 kPa) $ZnGeP_2$ (1.003g)	1311	1271	40	$ZnGeP_2$	3.99	173 hrs	6"
I-2 c Chemical HPVT	HCl (35 kPa) $ZnGeP_2$ (1.005g) Zn_3P_2 (44.6mg) P (21.7 mg)	1311	1271	40	$ZnGeP_2$	2.95	173 hrs	6"
I-3 c Chemical HPVT	HCl (35kPa) $ZnGeP_2$ (1.005g) P (51.5mg)	1311	1271	40	$ZnGeP_2$ Textured Sample	2.81	173 hrs	6"
III-2 Chemical HPVT	HCl (35kPa) $ZnGeP_2$ (1.1631g) Zn_3P_2 (3.8mg) P (47.1mg)	1301	1280	21	$ZnGeP_2$ ZnP_2 (5%) Zn_3P_2 :Ge(5%) Ge/GeP (1%)	~3	216hrs	Baked Out Carbonized 6"
III-3 Chemical HPVT	HCl (35 kPa) $ZnGeP_2$ (1.12338g) Zn_3P_2, (2.9mg) P (50mg)	1301	1280	21	$ZnGeP_2$ ZnP_2 (2%) Zn_3P_2 :Ge (5%) Ge/GeP (2%)	3.39	216hrs	Baked Out Carbonized 6"

(a)

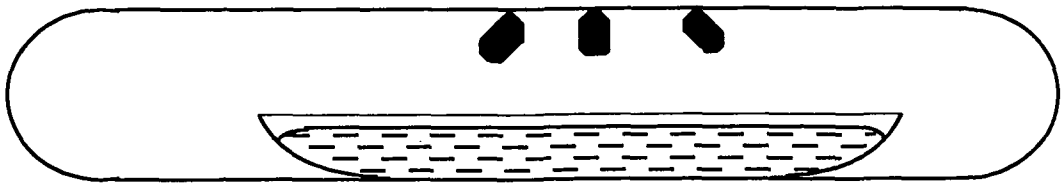

(b)

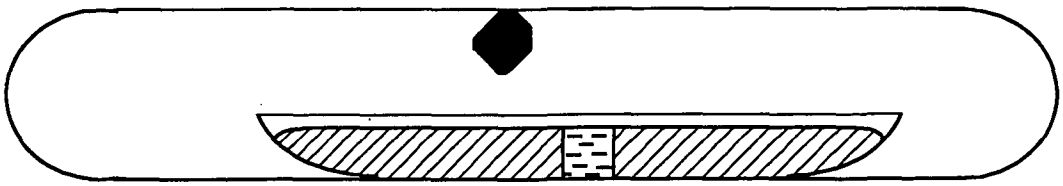

(c)

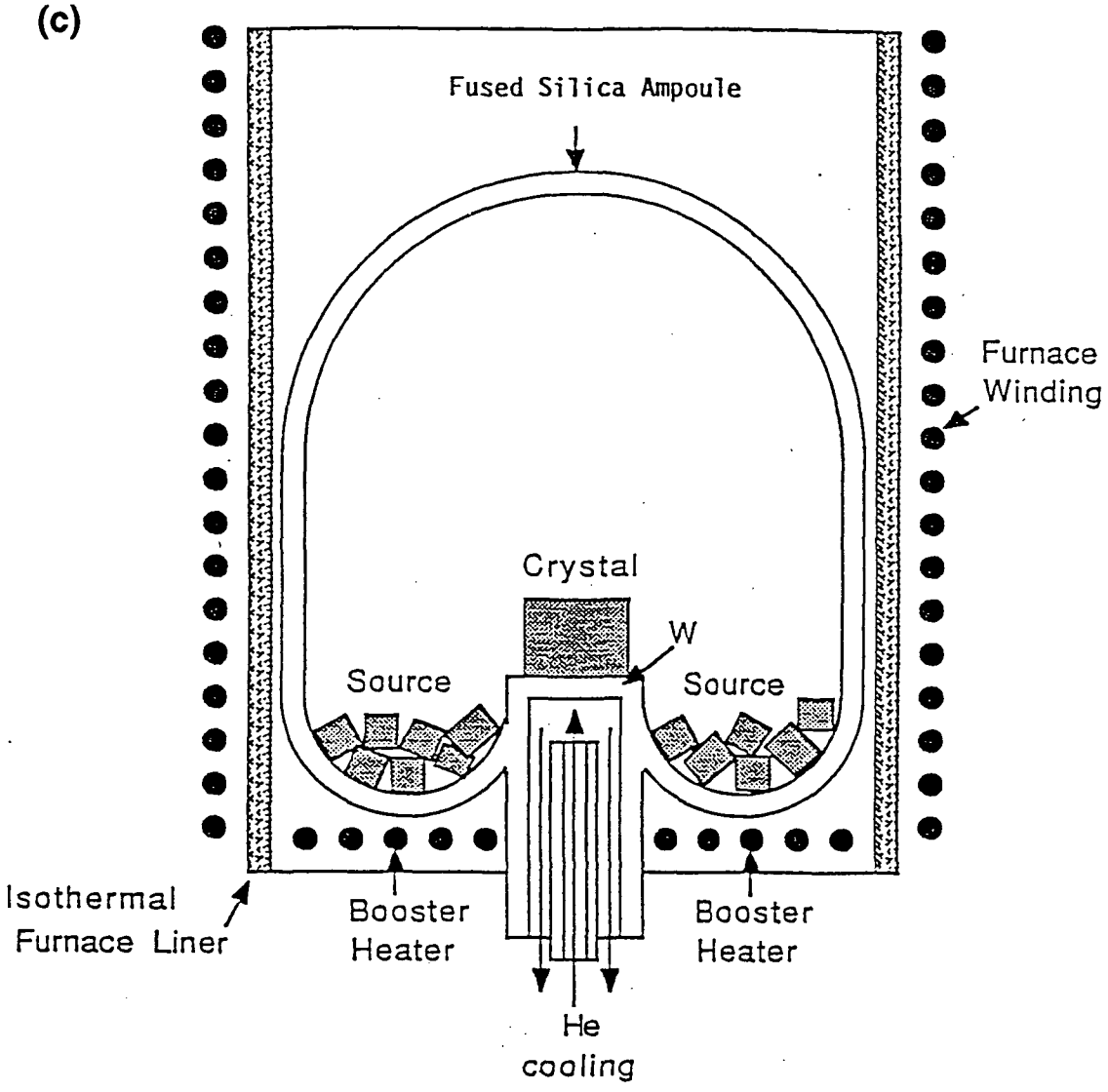
Fused Silica Ampoule
Furnace Winding
Crystal
W
Source
Source
Isothermal Furnace Liner
Booster Heater
Booster Heater
He cooling

(a)

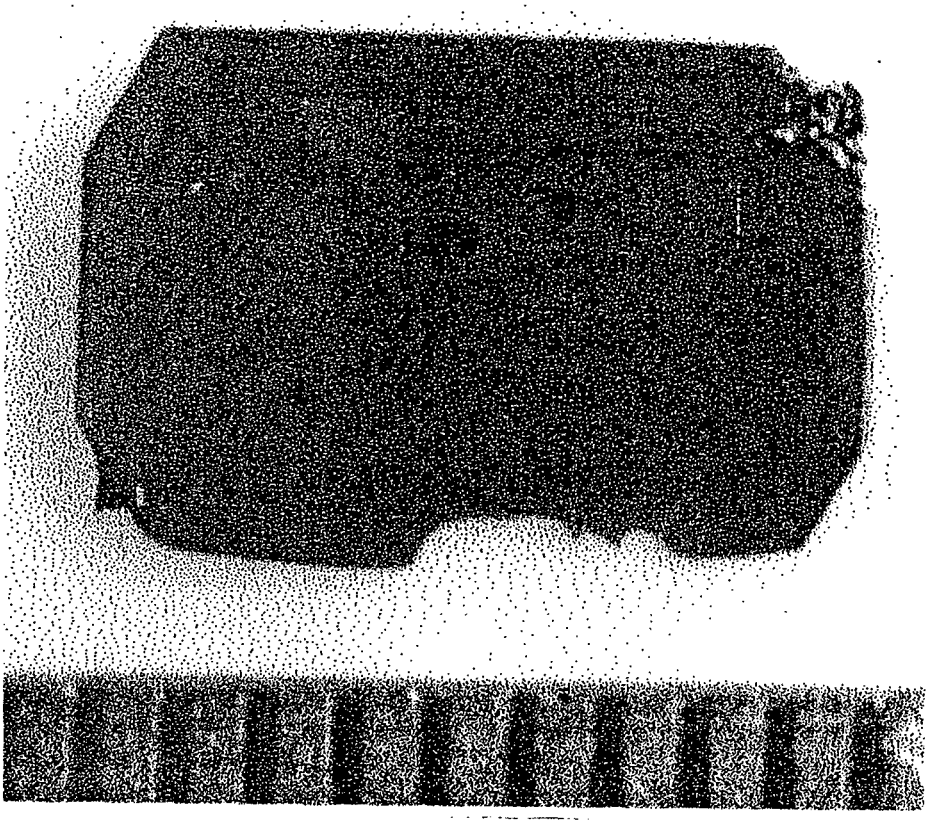

1 mm scale

(b)

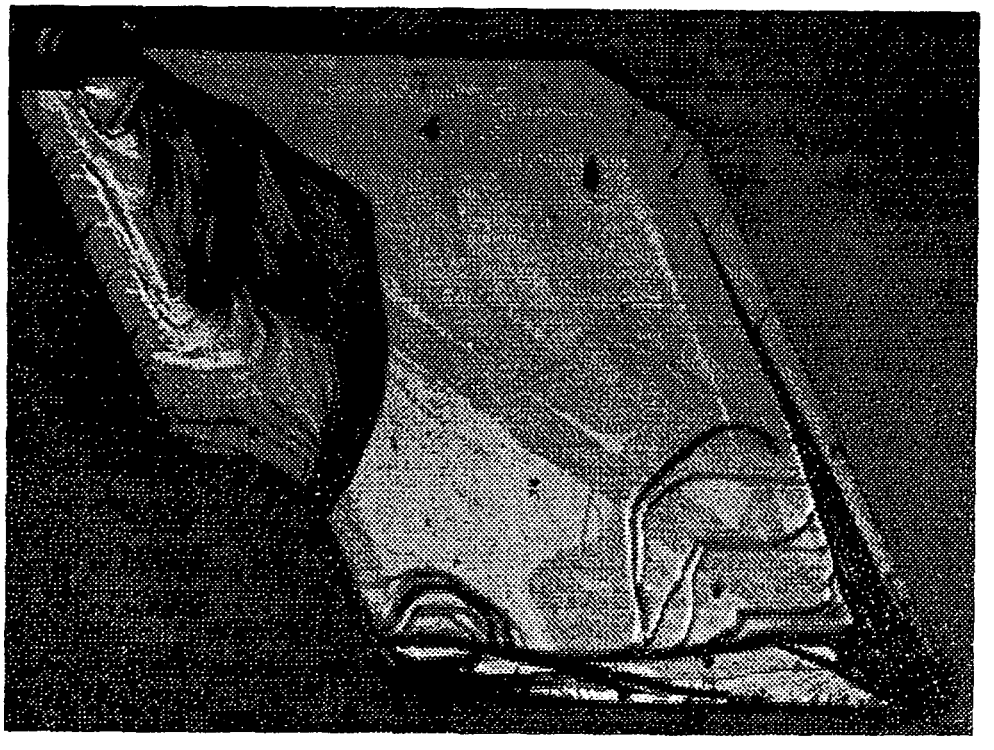

Figure 2. $ZnGeP_2$ Crystals grown by High Pressure Vapor Transport

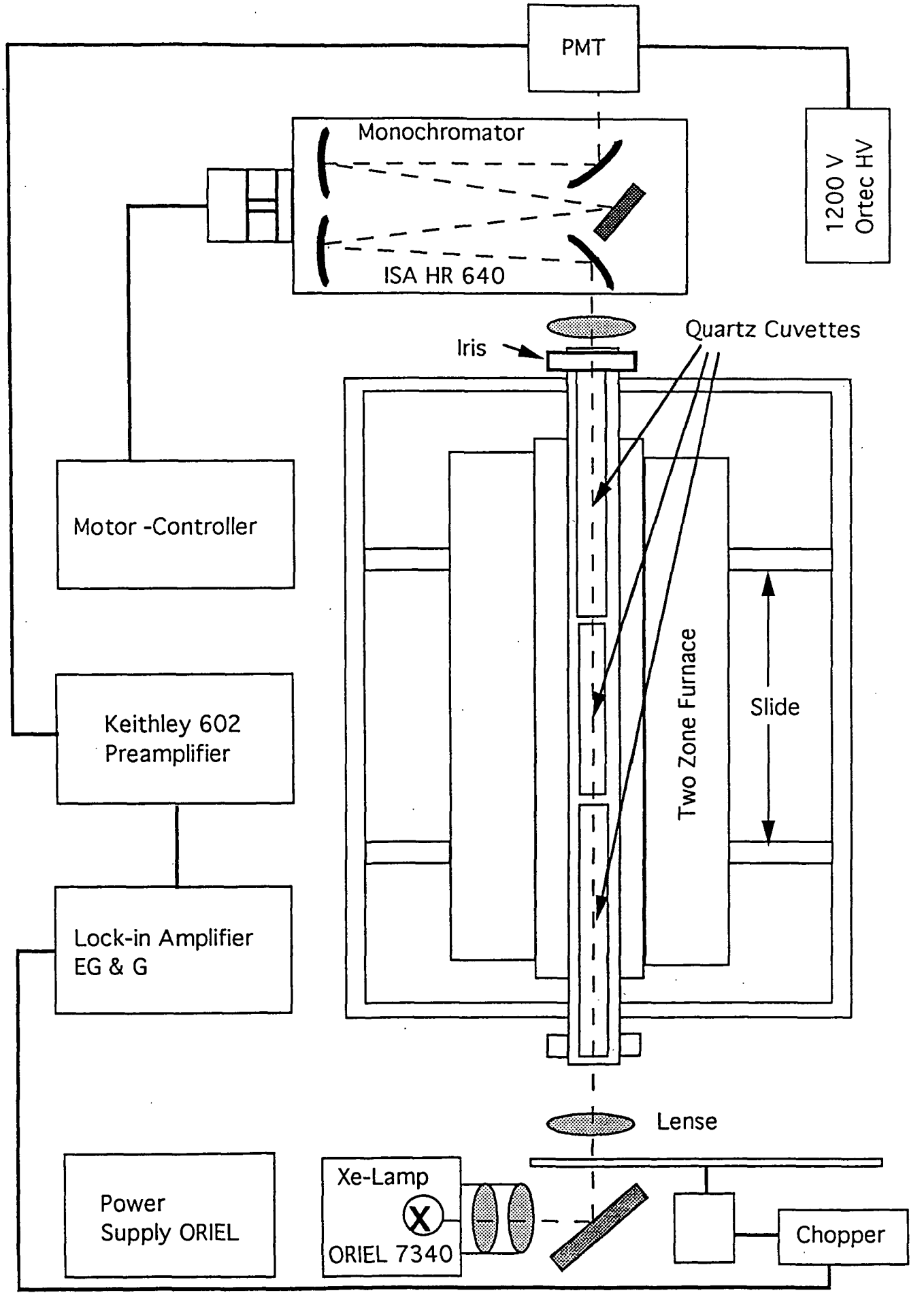

Figure 3. Schematic representation of the arrangement used in optical absorption measurements

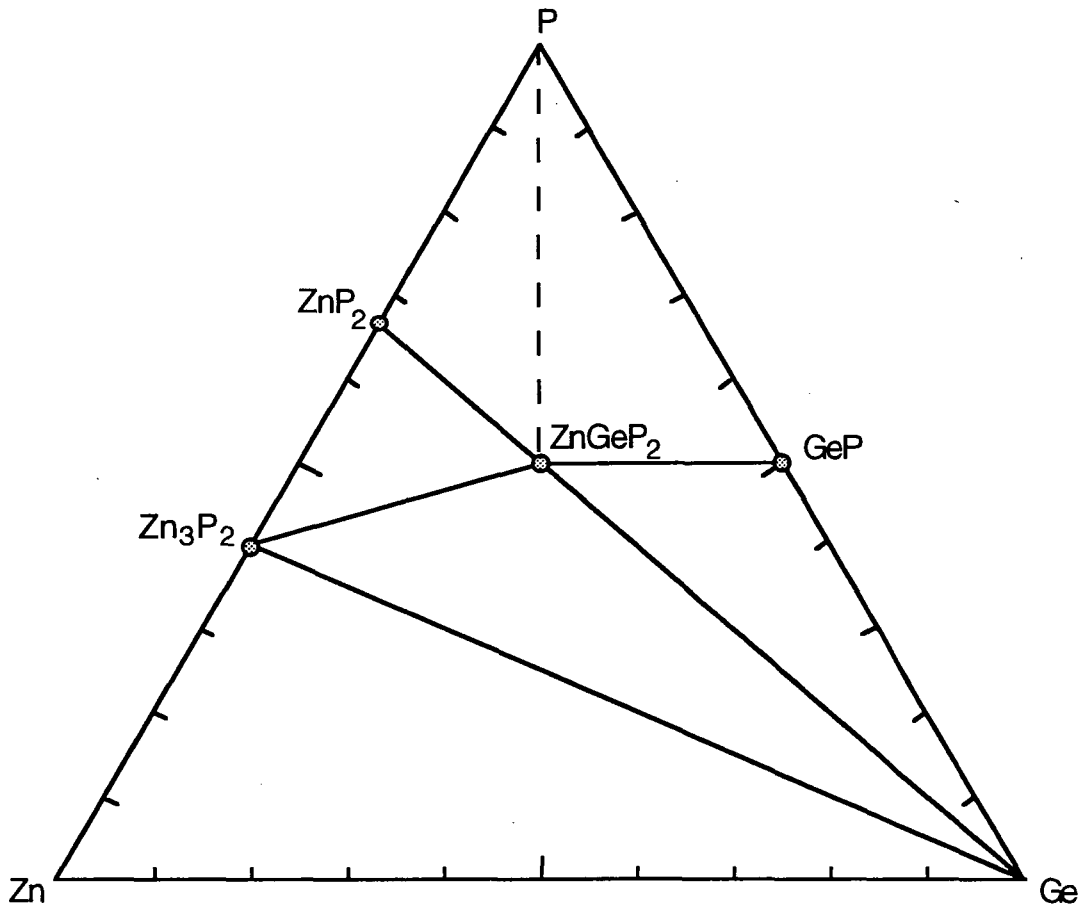

Figure 4. Gibbs Triangle for the Zn-Ge-P System

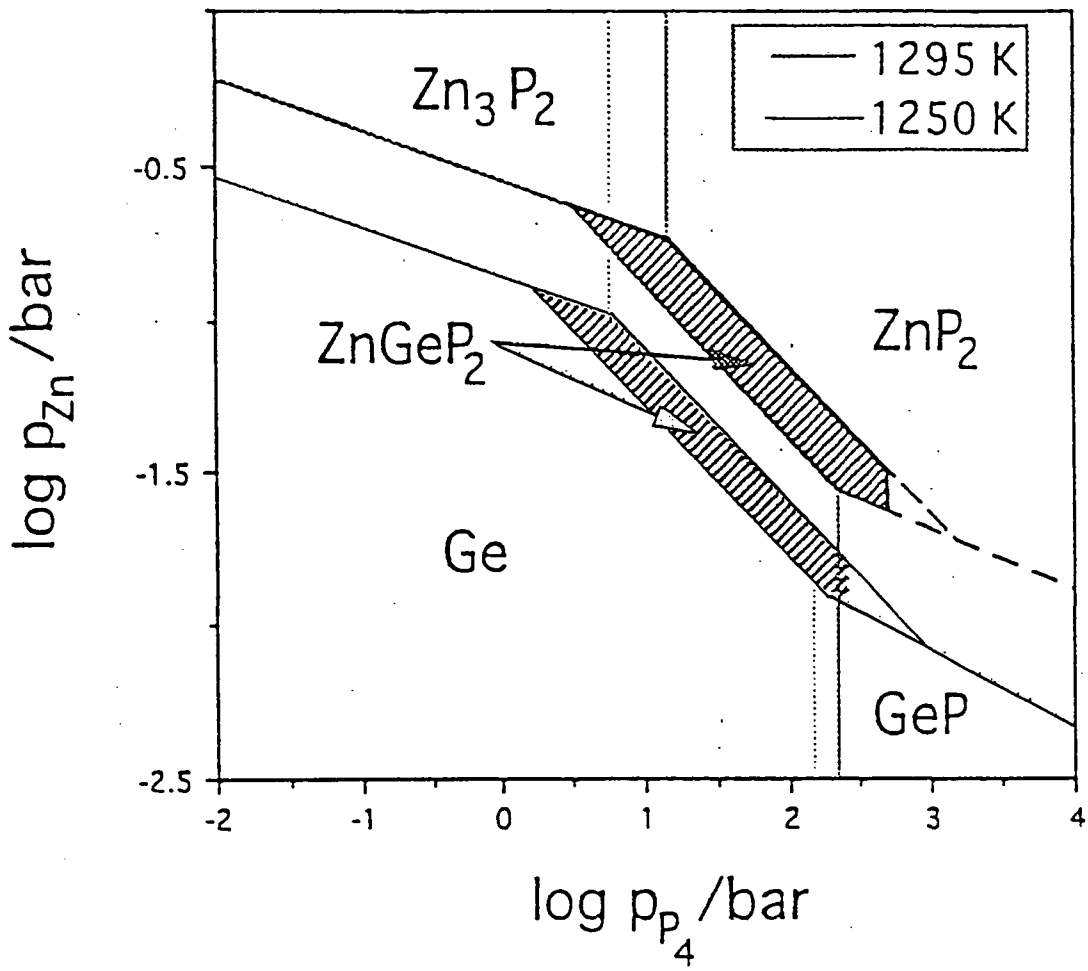

Figure 5. Predominance field for $ZnGeP_2$ at two temperatures[11].

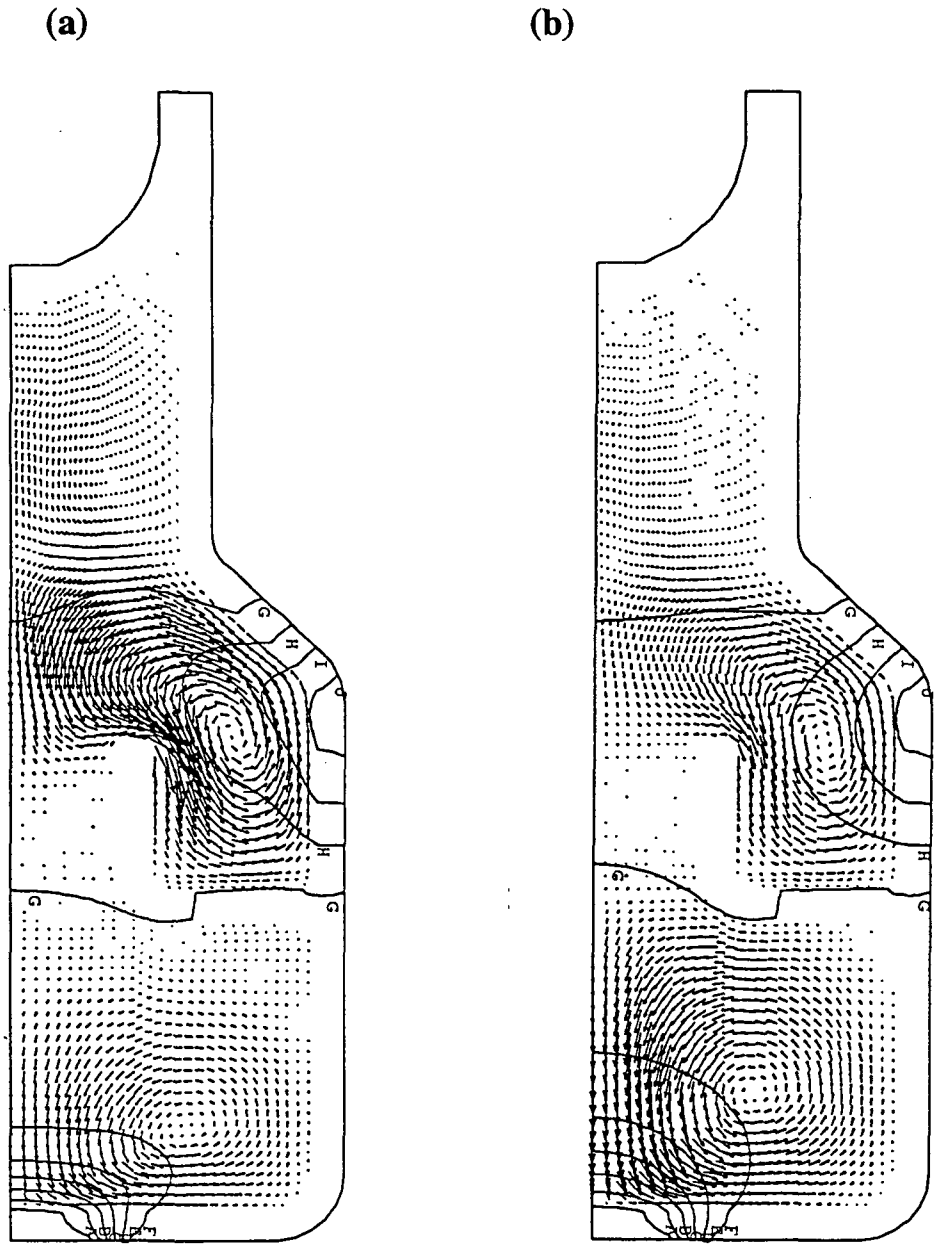

Figure 6. Calculated isotherms (solid lines A 1229K, B 1242K, C 1254K, D 1267K, E 1279K, F 1292K, G, 1304K, H 1317K, I 1329K, J 1342K) and flow (small arrows) for HPVT transport of $ZnGeP_2$ in a reactor of modified Scholz geometry. (a) 0.1 **g**, (b) 0.001 **g**.

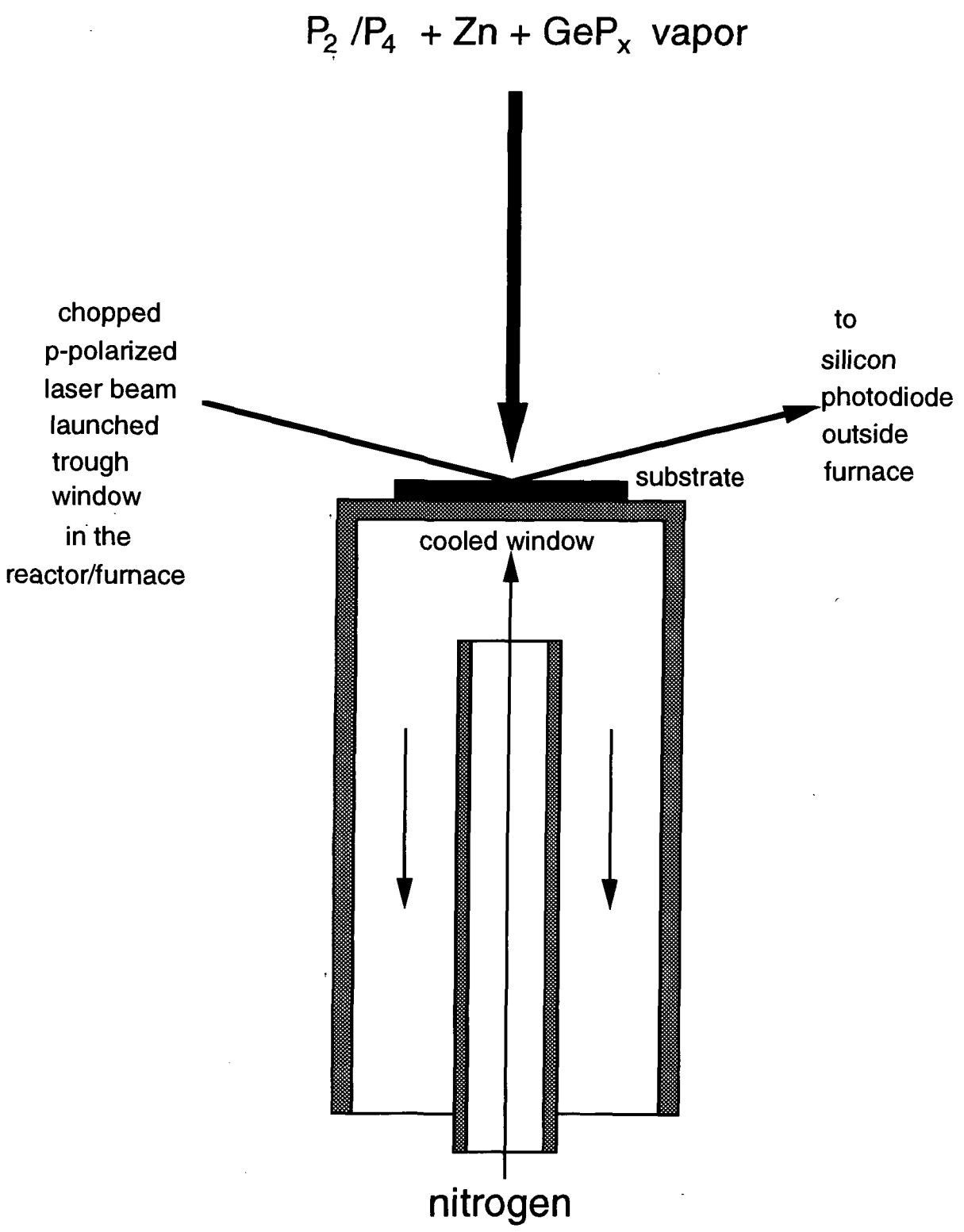

Figure 7. Schematic representation of the implementation of PRS under the conditions of HPVT in a reactor of modified Scholz geometry.

- angle of incidence is the Brewster angle of the Si-substrate
  (dielectric function $\varepsilon_{(\lambda=6328Å)} = (15.25 , 0.17)$ -> $\varphi_B = 75.637°$)
- p-polarizied light: $\lambda = 6328$ Å

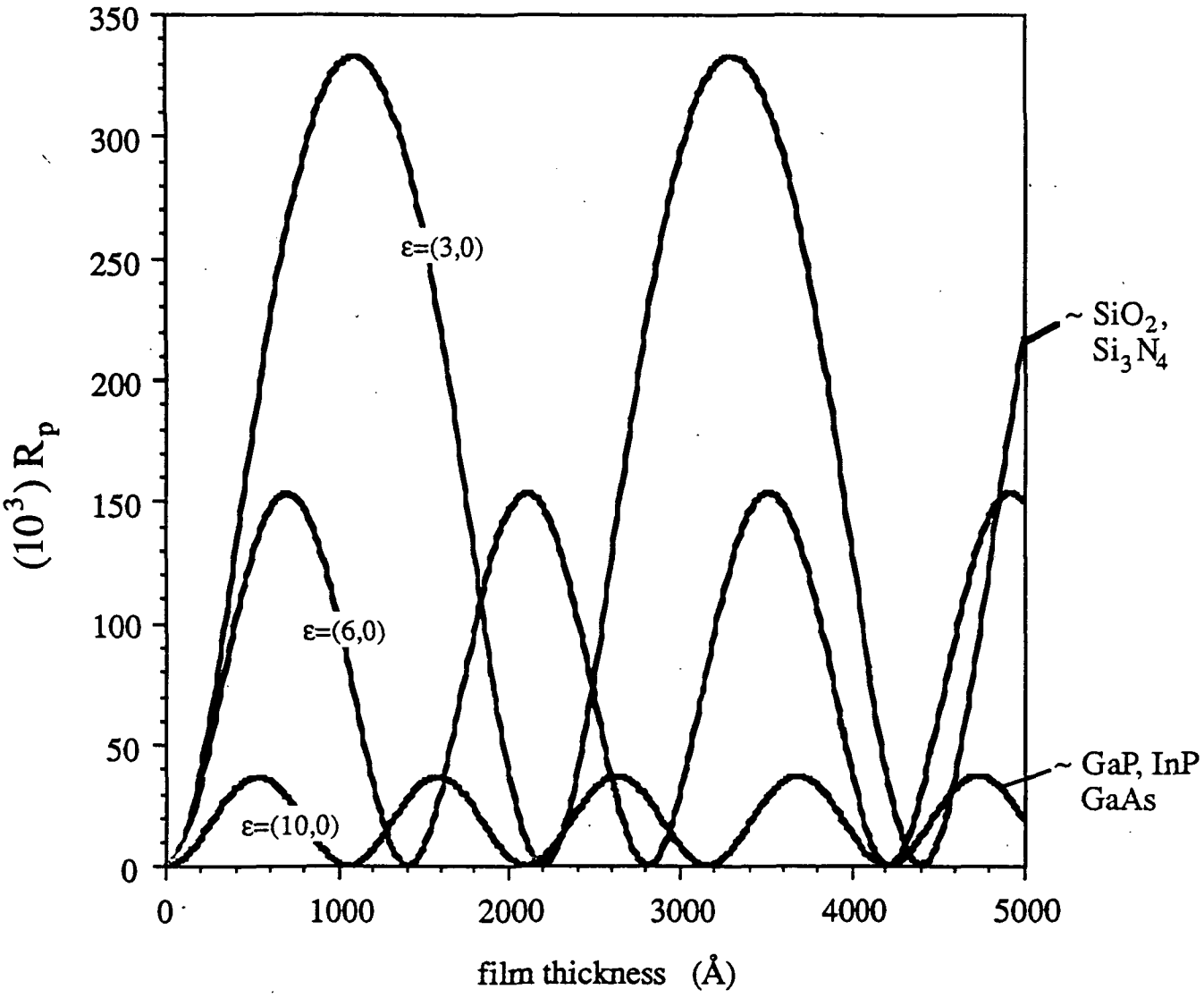

Figure 8. Simulation of the interference oscillations in the PRS intensity for the heteroepitaxial overgrowth of silicon for a selected dielectric constants of the epilayers

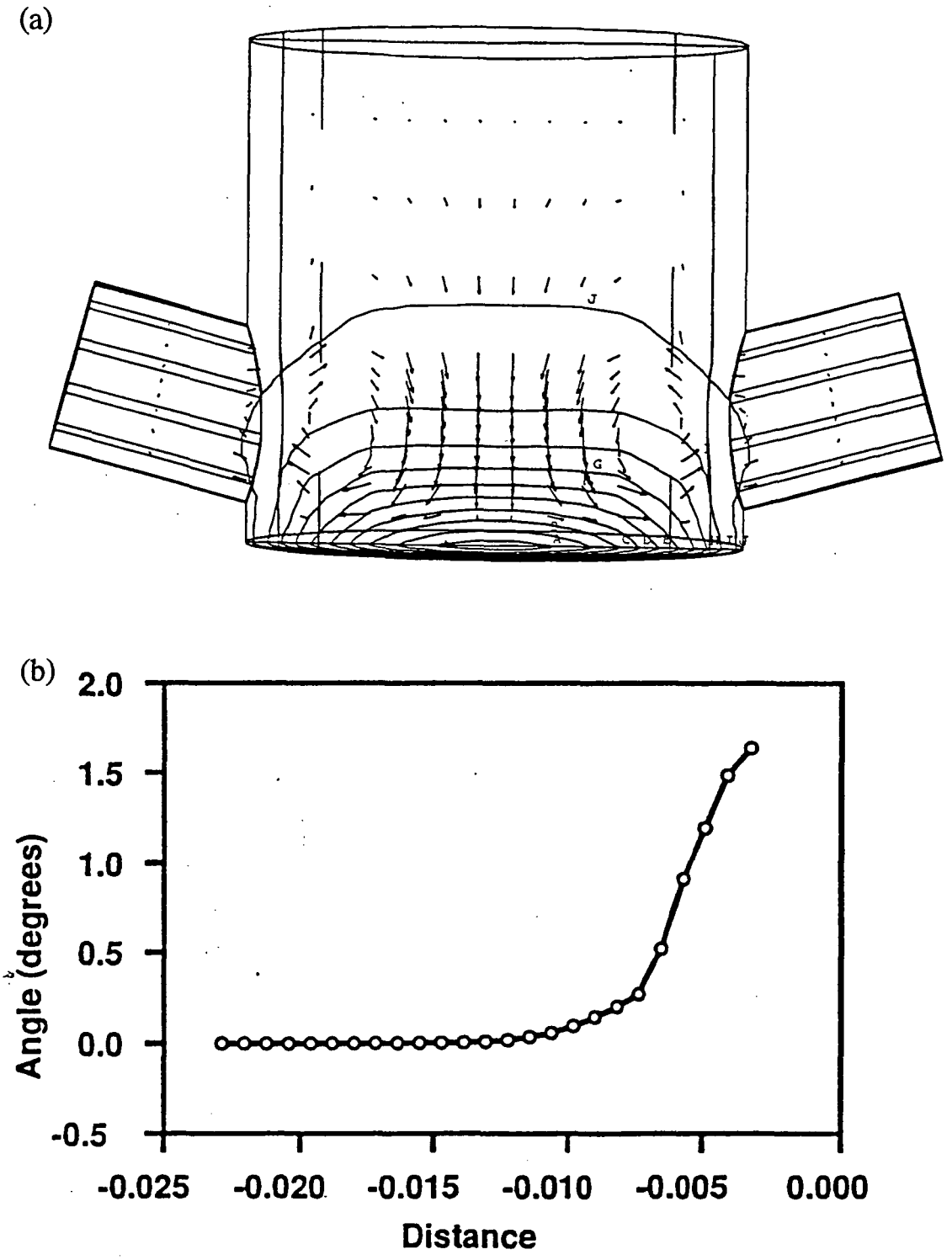

Figure 9. (a) Isotherms and flow velocity vectors for a close-space vapor transport ampule incorporating ports for p-polarized reflectance spectroscopy; (b) Deviations of the beam angle inside the growth ampule from normal incidence at the entrance window due to beam stirring in the vapor atmosphere

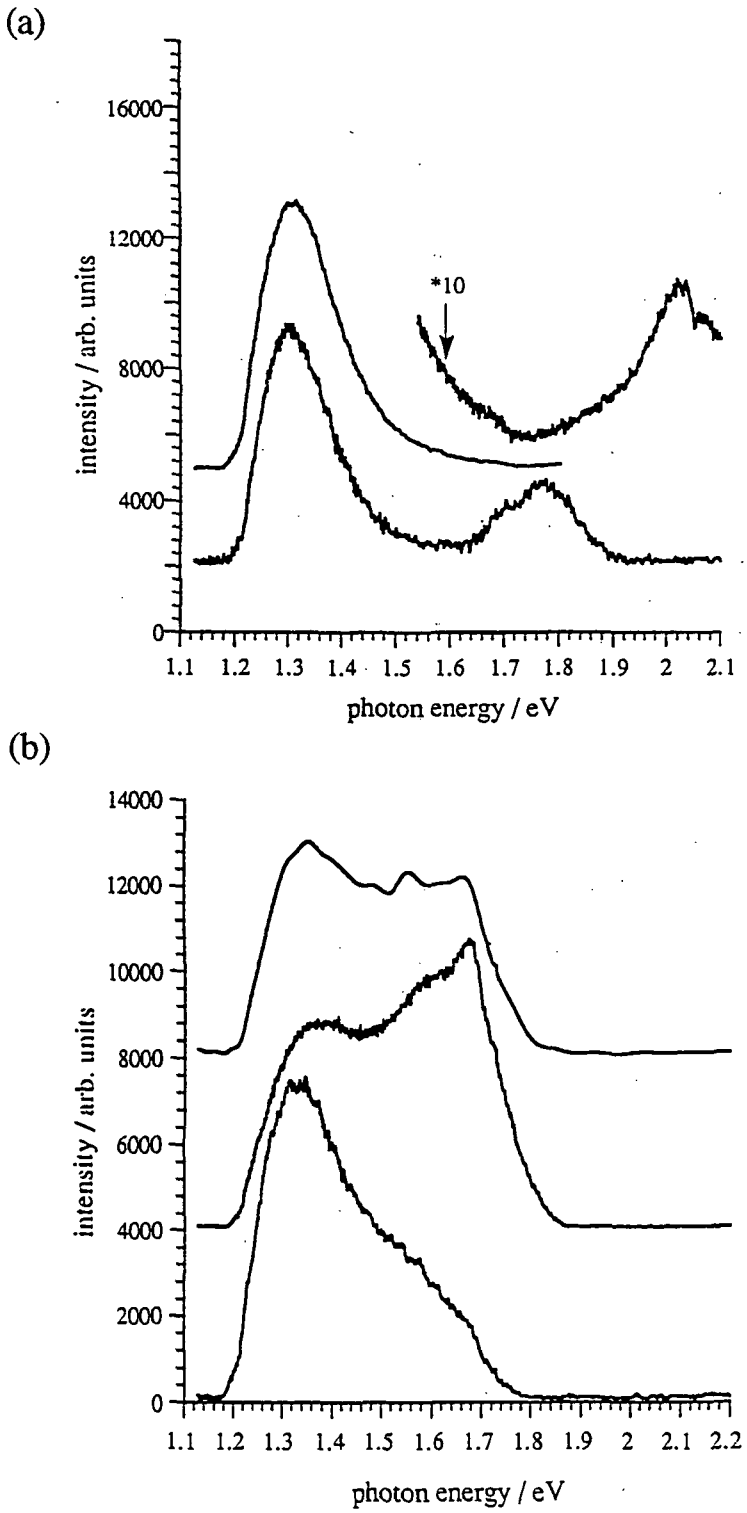

Figure 10. Photoluminescence spectra of $ZnGeP_2$: (a) Crystals grown by HPVT, (b) Crystals grown from the melt, top trace as-grown, middle trace annealed, bottom trace etched

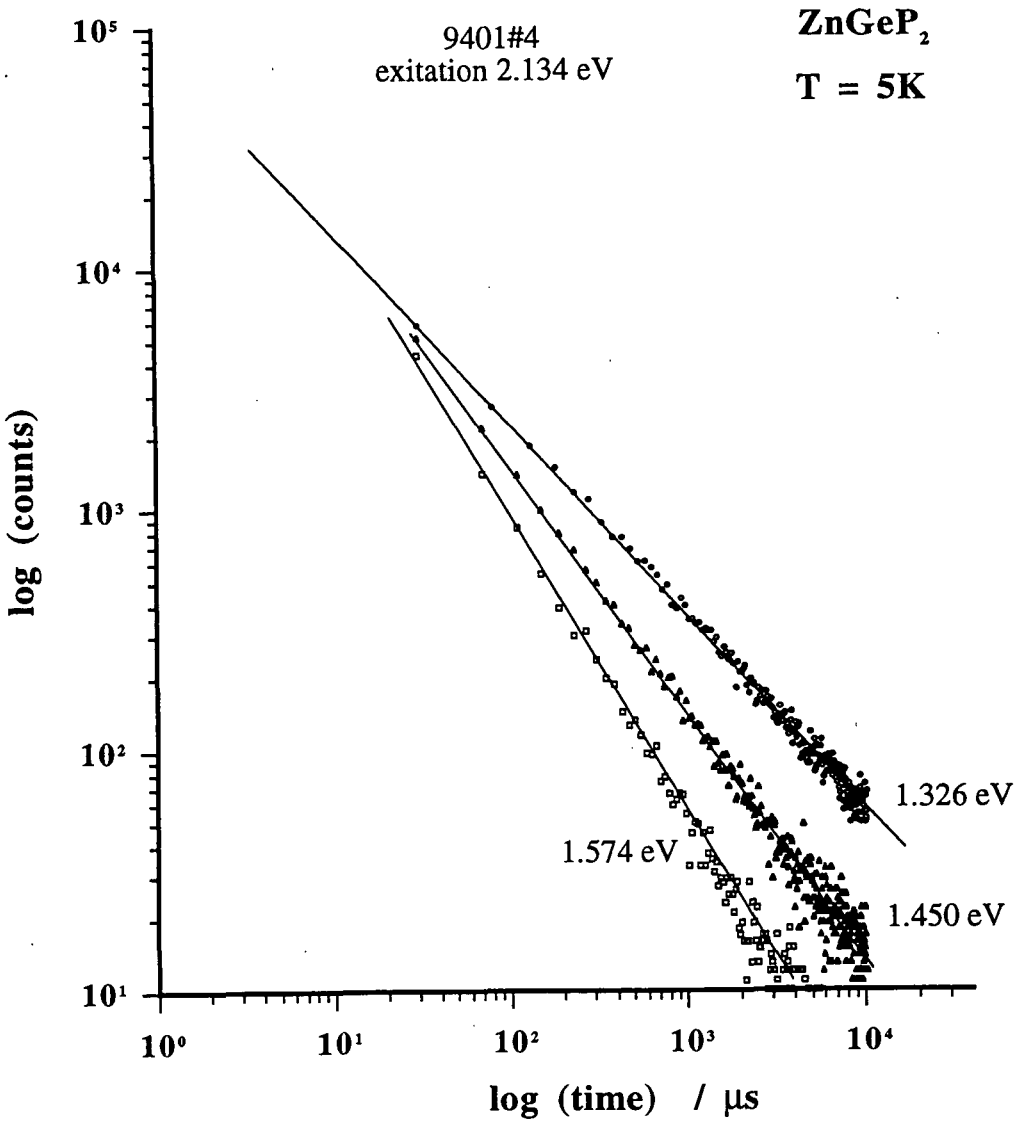

Figure 11. Time-dependence of the luminescense intensity for a crystal of $ZnGeP_2$ grown by directional solidification

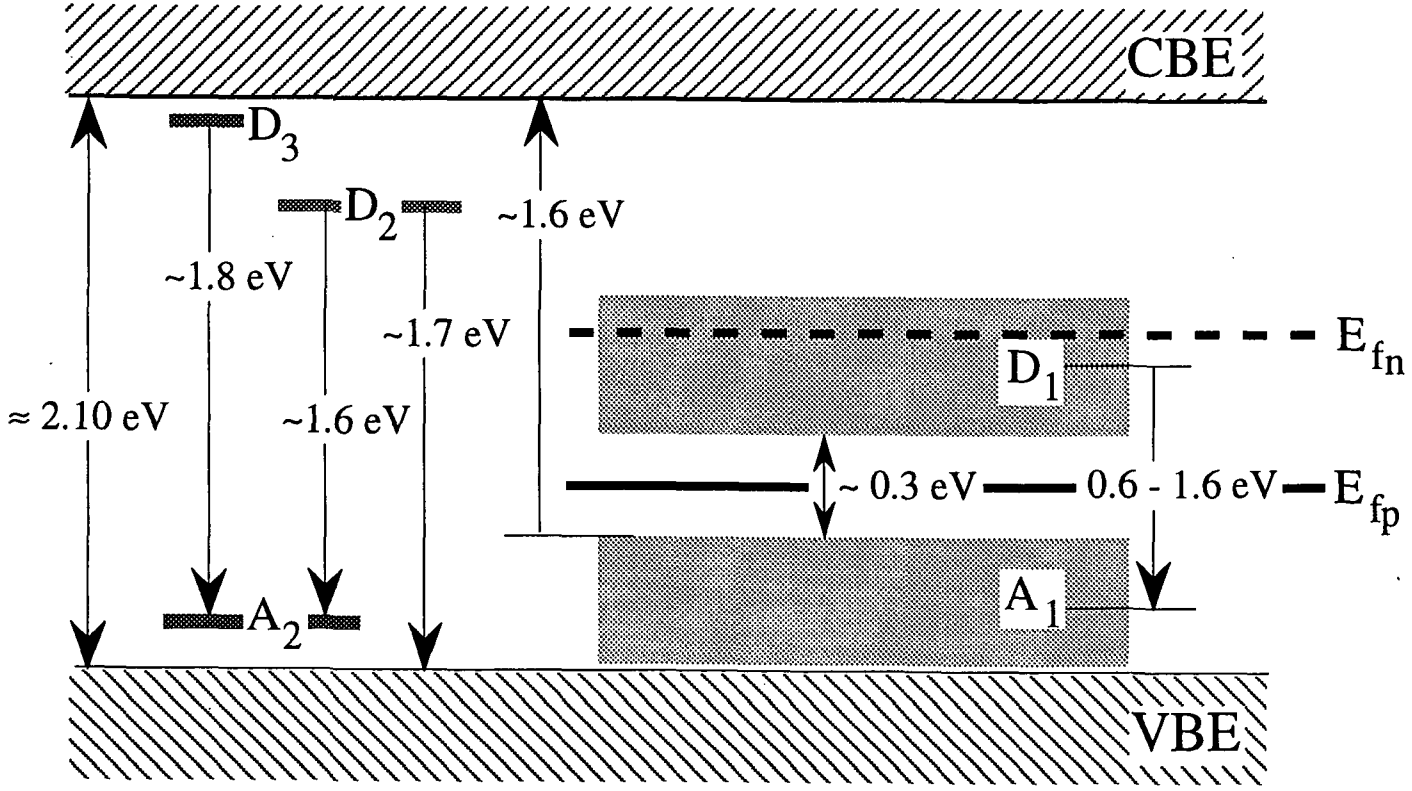

Figure 12. Interpretation of the observed optical behavior of $ZnGeP_2$ associated with various point defect related sub-bands and energy eigenvalues in the bandgap